# Modulation of leading edge vorticity and aerodynamic forces in flexible flapping wings

**Liang Zhao[1], Xinyan Deng[1,3] and Sanjay P Sane[2,3]**

[1] School of Mechanical Engineering, Purdue University, West Lafayette, IN 47907, USA
[2] National Centre for Biological Sciences, Tata Institute of Fundamental Research, GKVK Campus, Bellary Road, Bangalore 560 065, India

E-mail: xdeng@purdue.edu and sane@ncbs.res.in

## Abstract

In diverse biological flight systems, the leading edge vortex has been implicated as a flow feature of key importance in the generation of flight forces. Unlike fixed wings, flapping wings can translate at higher angles of attack without stalling because their leading edge vorticity is more stable than the corresponding fixed wing case. Hence, the leading edge vorticity has often been suggested as the primary determinant of the high forces generated by flapping wings. To test this hypothesis, it is necessary to modulate the size and strength of the leading edge vorticity independently of the gross kinematics while simultaneously monitoring the forces generated by the wing. In a recent study, we observed that forces generated by wings with flexible trailing margins showed a direct dependence on the flexural stiffness of the wing. Based on that study, we hypothesized that trailing edge flexion directly influences leading edge vorticity, and thereby the magnitude of aerodynamic forces on the flexible flapping wings. To test this hypothesis, we visualized the flows on wings of varying flexural stiffness using a custom 2D digital particle image velocimetry system, while simultaneously monitoring the magnitude of the aerodynamic forces. Our data show that as flexion decreases, the magnitude of the leading edge vorticity increases and enhances aerodynamic forces, thus confirming that the leading edge vortex is indeed a key feature for aerodynamic force generation in flapping flight. The data shown here thus support the hypothesis that camber influences instantaneous aerodynamic forces through modulation of the leading edge vorticity.

(Some figures in this article are in colour only in the electronic version)

## Introduction

Over the last two decades, diverse observations of natural flights have implicated the leading edge vortex as a primary contributor to aerodynamic force generation. Examples of these cases range from the flapping flight of insects (Ellington *et al* 1996, Srygley and Thomas 2002), birds (swifts, Videler *et al* 2004; hummingbirds, Warrick *et al* 2005) and bats (Muijres *et al* 2008) to the fins of fish (Lu and Shen 2008) and the dispersal flight of rotating plant seeds (Lentink *et al* 2009).

A common feature in these diverse examples of the flapping or rotary motion of the airfoils is the presence of a prominent vortex along the leading margin of the airfoil. A similar leading edge vortex is also present in the case of airfoils translating at moderate angles of attack ($>13.5°$, Dickinson and Gotz 1993), but it grows in size and detaches as the wing translates and is eventually shed in the wake. This leads to separation of flow and rapid loss in lift—a phenomenon familiar in the classical aircraft literature as 'stall' (e.g. Acheson 1990).

Using mechanical flappers, several papers (e.g. Ellington *et al* 1996, Dickinson *et al* 1999) have shown that flapping or rotary airfoils are able to generate stable forces at high angles of

---

[3] Authors to whom any correspondence should be addressed.

attack and consequently their aerodynamic performance was significantly better than the corresponding fixed wing case (for a review, see Sane 2003). Moreover these experiments also indicated the presence of strong leading edge vorticity on the flapping wing but the magnitude of this vortex was smaller and more stable than its fixed wing counterpart—similar to the corresponding aerodynamic forces generated by these airfoils. These observations were further confirmed by detailed flow measurements on mechanical flappers (Birch and Dickinson 2001, Lentink *et al* 2009) indicating that leading edge vortices may indeed play a key role in enhancing the aerodynamic effectiveness of a flapping or rotary wing. However, to test the hypothesis that leading edge vortices determine aerodynamic force generation, it is necessary to alter the leading edge vorticity independently of the gross motion of the wings while also measuring the corresponding changes in the aerodynamic forces.

In this study, we varied the flexural stiffness of the wing margin to subtly alter the flexion of the wings during flapping, and directly measured the resultant flows using digital particle image velocimetry (DPIV) and aerodynamic forces using force transducers. These data provided us with a comprehensive and quantitative picture of the influence of trailing edge flexion on leading edge vorticity as well as the aerodynamic forces on flapping wings.

## Materials and method

### Force measurements

The dynamically scaled mechanical flapper used here has been previously described in detail in Zhao *et al* (2010) and will be only briefly described here. The flapper was equipped with a six component force sensor (ATI NANO-17, Apex, NC, USA) at the base of the wing to measure instantaneous aerodynamic forces normal and parallel to the wing surface. The motion of the wings could be driven along three orthogonal Euler angles through a bevel-geared transmission actuated through coaxial drive motor shafts. Three 16 mm, 0.3 Nm torque dc brush motors (Maxon, Sachseln, Switzerland) powered the drive shafts. A set of magnetic encoders embedded in the motors provided kinematic feedback and ensured fidelity of the desired kinematic pattern (figure 1(*a*)). The non-dimensional force coefficients were calculated using the equation

$$C_F = \frac{F}{\frac{1}{2}\rho U_t^2 S_1 \cdot \hat{r}_2^2(S)}, \quad (1)$$

where $\rho$ is the density of fluid, $U_t$ the path velocity of wing tip and $F$ is either lift (*L*), drag (*D*) or net force (*N*) (for conventions, see Sane and Dickinson (2001)). The experiments reported here were carried out at Reynolds numbers of about 2000, as calculated from the equation

$$\bar{Re} = \frac{\bar{b}\bar{U}_t}{\nu} = \frac{4\theta R^2 n}{\nu(\text{AR})}. \quad (2)$$

In this equation, $\bar{b}$ is the mean chord length, $\bar{U}_t$ is the mean wing tip velocity, AR is the aspect ratio, $n$ is the wing beat frequency, $R$ is wing length, $\theta$ is the wing beat amplitude

**Table 1.** Material and aerodynamic information of models.

| Models | Thickness (mm) | EI (Nm$^2$) |
|---|---|---|
| Polyes0.002 | 0.05 | 4.39E-6 |
| Polyes0.003 | 0.075 | 1.01E-5 |
| Polyes0.005 | 0.125 | 3.24E-5 |
| Mylar0.007 | 0.175 | 2.15E-4 |
| PETG0.06 | 1.47 | 8.23E-4 |

(peak-to-peak in radians) and $\nu$ is the kinematic viscosity of the fluid (Ellington 1984a, 1984b). These Reynolds numbers are typical of larger insects such as moths and butterflies in which wing flexion is significant.

Using this system, we generated aerodynamic polar plots for a suite of five wings with flexural stiffness ranging from $4.39 \times 10^{-6}$ to $8.23 \times 10^{-4}$ N m$^{-2}$. The flexural stiffness, EI, for these studies is given by the following equation (Gordon 1978):

$$\text{EI} = Fw^3/(3\delta) \quad (3)$$

where the applied force is $F$, the wing tip displacement is $\delta$ and chord length of the wing is $w$.

These wings are a subset of the 16 wings used in an earlier study (Zhao *et al* 2010; table 1), but encompasses the same range of flexural stiffness values. The choice of the wings used in this study was dictated primarily by the need to explore a flexion range that is wide enough to capture the key flow phenomena but restricted enough to ensure that there is no redundancy in the conclusions.

### Flow visualization using particle image velocimetry

To complement the force measurements of flexible flapping wings, we used a custom continuous-laser DPIV system to visualize the instantaneous flows and measure the velocity fields around the moving wing. The wing materials were clear, smooth in surface and even in thickness, which ensured the consistency of laser sheet strength and direction. We seeded the flow with air bubbles pumped out of a porous ceramic filter within the oil tank (see Sane 2001 or Birch and Dickinson 2001 for a description of a similar system). To maintain low noise levels in the flow, we conducted the experiments after the large bubbles rose to surface leaving behind only small and relatively neutrally buoyant bubbles in the oil. The size of the bubble is wide spread in a range from 10 to 50 $\mu$m with the medium-sized bubble being around 20 $\mu$m. To calculate the error of the PIV, we measured the velocity of the wing model and compared it with the velocity output from PIV system. For a 22 cm s$^{-1}$ wing velocity, the PIV results showed a value of 20.40 cm s$^{-1}$. From this we estimated the error to be about 7%.

The oil filled with small bubbles was then illuminated using a 2D sheet of continuous 8 W Argon–Ion laser (Coherent Inc., Santa Clara, CA; wavelength = 457–514 nm, figure 1(*b*)). The laser beam emerging from the source was reflected at right angles by the flat mirror and passed through a cylindrical lens to obtain a 2D sheet. The light sheet illuminated a 2D section of the oil with bubbles, which was imaged using a high-speed camera (Photron 1024; resolution 1024 × 1024
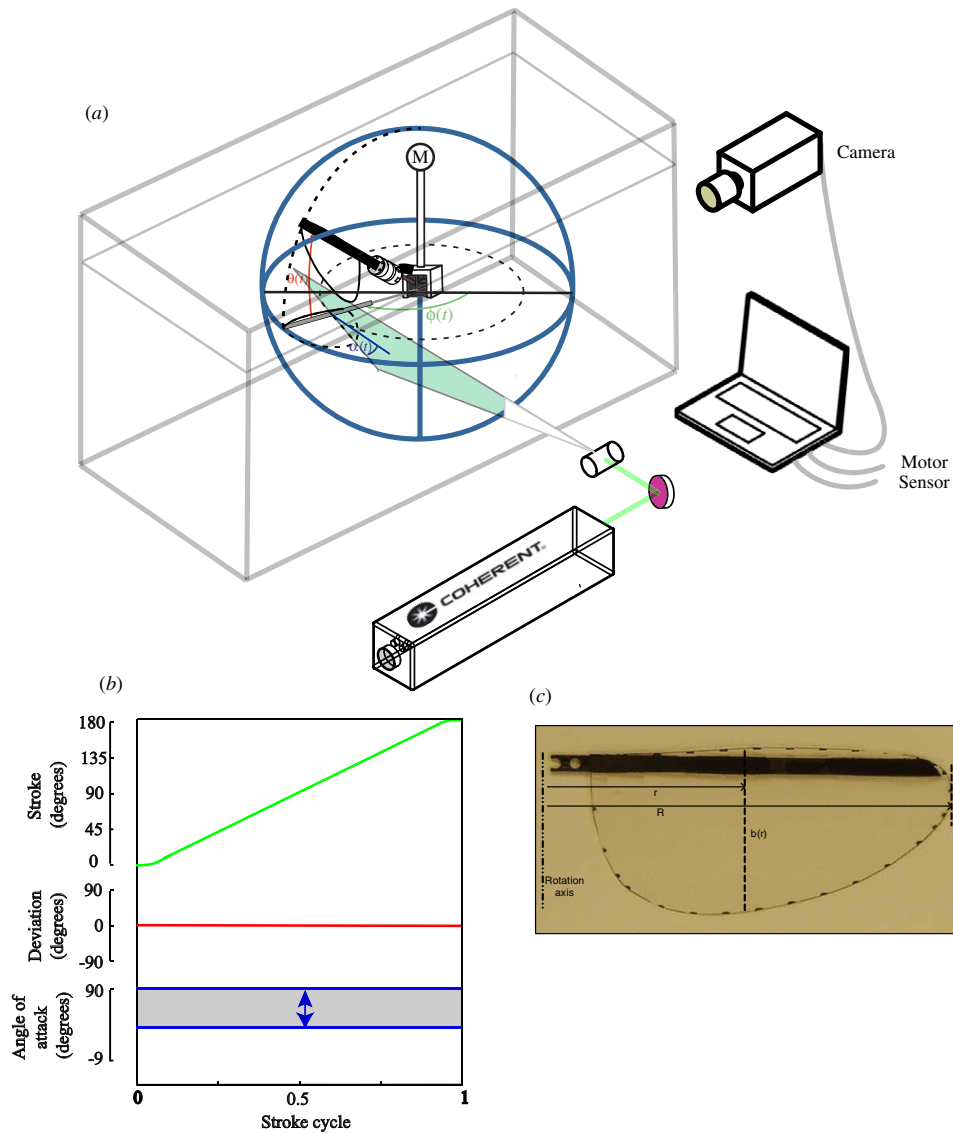
**Figure 1.** Experimental setup. (*a*) Diagram of the experimental apparatus. A computer controls the three stepper motors ('M' represents three motors) along three degrees of freedom thus enabling motion in any arbitrary 3D kinematics pattern. A high power continuous laser adjustable by a mirror (violet) passes through a cylindrical lens to form a continuous laser sheet to illuminate the ambient fluid around the cross-section of the wing. The flow, seeded with air bubbles generated from the ceramic filter (not shown), is imaged with a high-speed camera facing the laser sheet. A 6D force sensor at the base of the model wing measures the instantaneous force and moments on the wing. (*b*) The kinematics applied on the wing models during the experiments. In the experiments described here, the wing revolved uniformly at an angle of attack of $45°$. After starting impulsively, the model reached the constant angular speed over its $180°$ stroke. (*c*) Representative wing model. The mean chord length is 45 mm, and the wing length is 100 mm. The surface area of each wing equals 3370 mm$^2$. The Reynolds number for our experiments was calculated at 2000.

pixels; 500 frame s$^{-1}$) fitted with a 60 mm fixed lens (Nikon) oriented perpendicular to the laser sheet. Successive frames of the high-speed video, which captured the flow reported by the changing bubble configuration from frame to frame, were quantified using a MATLAB-based toolkit, MATPIV, developed specifically for analysis of PIV data.

## Results

### *Measurement of forces*

We calculated the lift, drag and net force coefficients (equation (1)) on five models, chosen as a subset of the 16 wings described in Zhao *et al* (2010). For ready reference, the aerodynamic polars of these five wing models are shown in figure 2(*a*). In the experiments described here, these wings were actuated to revolve in a horizontal plane at fixed angles of attack of $45°$ and the lift (red line), drag (green line) and net (blue line) force coefficients of these models were measured as a function of flexural stiffness. All force coefficients monotonically increased with increasing flexural stiffness. A rigid wing translating at angles of attack of $45°$ is expected to experience identical lift and drag coefficients due to the identical decomposition of net force vector into its orthogonal components. Expectedly, for flexible wings (i.e. with lower flexural stiffness values), lift and drag coefficients were
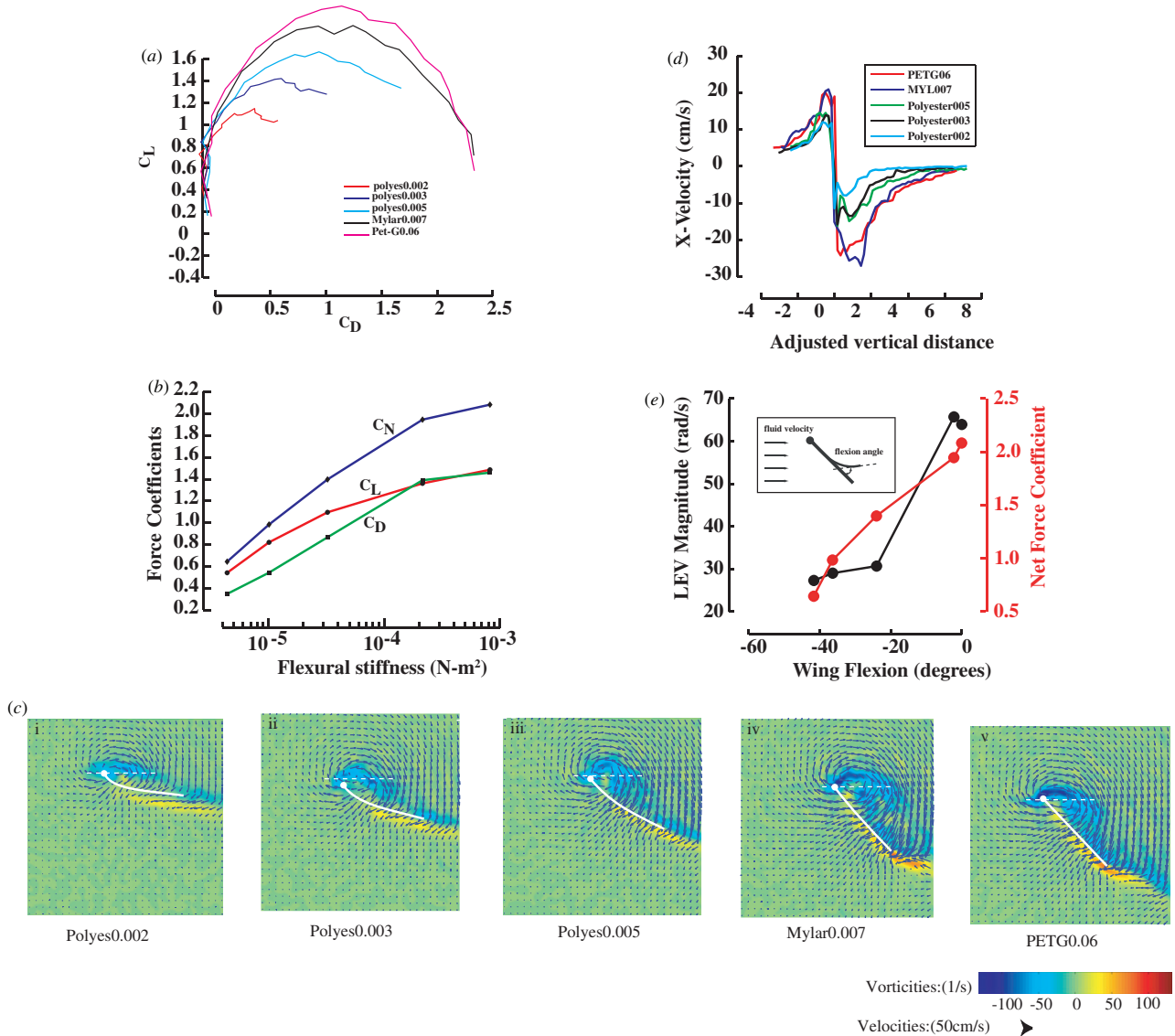
**Figure 2.** (*a*) Aerodynamic polar plots for the five wings. These plots are subsets of the plots in Zhao *et al* (2010) and highlighted here for convenience. These are models are given the names polyes0.002; polyes0.003; polyes0.005; Mylar0.007; PETG0.06. (*b*) Force coefficients of lift, drag and net force as function of flexural stiffness. (*c*) Leading edge vortices on the model wings. The white lines trace the cross-section of model wing at mid-stroke. In these plots, blue represents the vorticity of negative sign (clockwise), and the red one for the positive (counter clockwise). The velocity is also shown by the vectors. The vector length represents the magnitude of velocity. The results were tested at the maximum chord of the models. The strength of the mean value of the top ten vorticity cells have been shown below each panel. (*i*) polyes0.002; (*ii*) polyes0.003; (*iii*) polyes0.005; (*iv*) mylar0.007; (*v*) PETG0.06. (*d*) Change in X-velocity around the leading edge vortex. The equal rise and fall of velocity around the leading edge vortex indicates the presence of rolled-up vorticity. The X-velocity was measured through a horizontal cross-section through the vortex core. The zero-crossover in these plots indicates the presence of true vortex core. The lines are color coded (in order of decreasing flexural stiffness) such that red indicates the stiffest (PETG0.06), followed by dark blue (mylar0.007), green (polyes0.005), black (polyes0.003) and light blue (polyes0.002). (*e*) Magnitude of leading edge vorticity (black) and net force coefficient (red) as a function of wing flexion. (Inset) The definition of flexion angle: amplitude represents the angle between the leading edge tangent and the trailing edge tangent, and the minus sign means flexion and plus sign means camber. (Main figure) Force coefficients and LEV strength change monotonically as flexion angle changes for angles of attack of 45°. In both cases, the vorticity of the leading edge is maximum for a rigid wing and decreases as the flexion angle magnitude increases.

unequal due to wing flexion, but their values were comparable at greater wing flexural stiffness. As the wing flexural stiffness increased, their values reached plateau (figure 2(*b*)).

*Measurement of flows*

To quantify the effect of wing flexion on aerodynamic flows, we simultaneously measured the degree of flexion,

aerodynamic forces and flows as a function of changing angles of attack and flexural stiffness (figures 2(*c i–v*), (*e*)). Using 2D DPIV, we quantified both the velocity and vorticity flow fields around the maximum chord section (45 mm) of each of these five wing models revolving at 45° angles of attack. For the vorticity calculations, we maintained the standard convention of counter clock-wise rotation as positive. In each case, we
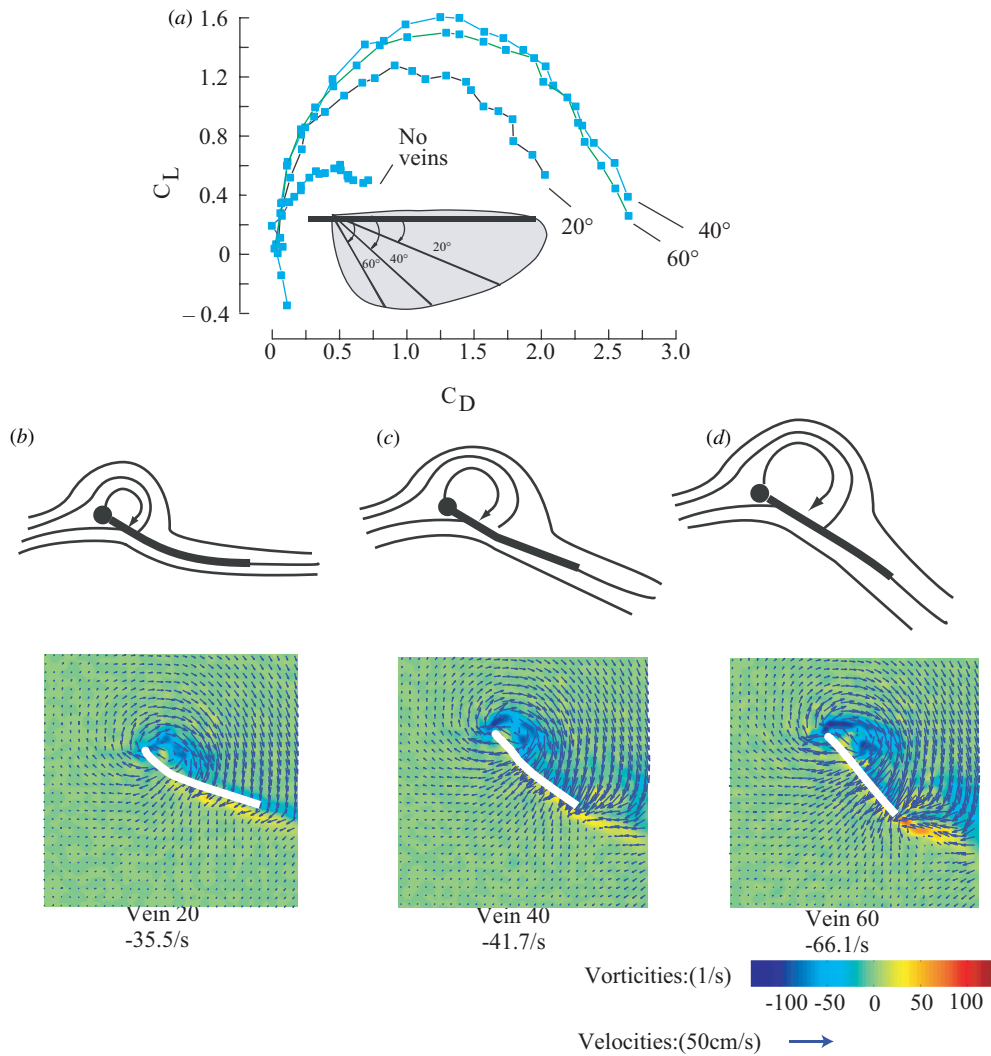
**Figure 3.** Altering wing flexion through wing venation. (*a*) Aerodynamic polar plots of wing with a leading edge spar and one of three vein configurations. The veins are either absent or placed at either 20°, 40° or 60° with respect to the leading edge spar. The vein placement enabled us to flex the wing through various angles. The corresponding flows for 20° (*b*), 40° (*c*) or 60° (*d*) venation are shown along with a cartoon representation of the associated flows. The numbers under each figure represent the maximum value for leading edge vorticity, which is negative because the leading edge vortices are clockwise. Reproduced from Zhao L *et al* 2010 Aerodynamic effects of flexibility in flapping wings *J. R. Soc. Interface* **7** 485–97

observed an attached leading edge vortex as the dominant feature of the flow field (figure 2(*c i–v*)) in agreement with previous experiments (e.g. Ellington *et al* 1996, Birch and Dickinson 2001) and computations (e.g. Liu and Kawachi 1999, Ramamurti and Sandberg 2002). To confirm that these structures were indeed vortical, we measured their velocity along a horizontal section through the core of the vortex for each wing. In each case, the velocity rises left of the core and falls to an equal degree toward the right of the core, characteristic of a rolled-up vortex (figure 2(*d*)). Moreover, the peak-to-peak values of these vortices varied directly as their flexural stiffness, thus confirming that the magnitude of the leading edge vorticity depends on the degree of flexion in these wings.

In the above described experiments, it is important to note that the main variable is flexural stiffness (EI) but not directly the wing flexion. Rather, the magnitude of wing flexion is set by the combination of flexural stiffness and its

aeroelastic interaction with its fluid medium. In each case, the wing flexion attained a steady value by the time the wing had traversed through an arc of 90°, and hence it was possible to assign a steady flexion value to the revolving wing. We defined the magnitude of flexion as the angle subtended between the tangents at the leading and trailing edges (inset, figure 2(*e*)).

Although shear layers were visible on the upper and lower surface of the airfoil, very little vorticity was shed into the wake from the trailing edge of the wing suggesting that the flow reattaches at the trailing edge even for these large angles of attack in a revolving wing. As a measure of the magnitude of leading edge vorticity, we calculated the average of the ten maximum values of vorticity in a specific interrogation region defined by the extent of the velocity plot in figure 2(*d*) around the leading edge. This average value provided a criterion that combined both the maximum and average vorticity of the leading edge vorticity, thus enabling a direct comparison between these magnitudes under different

experimental conditions. Both the magnitude of leading edge vorticity and the net force coefficients increased as the flexion decreased (figure 2(*e*)). Because the wing flexion in these experiments was not under experimental control but resulted from aeroelastic interactions between the moving flexible wing and the surrounding fluid, it was not possible to preset values of flexion between −20° and 0°, or derive an empirical functional relationship of the dependence of leading edge vorticity on flexural stiffness. Nevertheless, the present analysis allows us to conclude that the leading edge vorticity monotonically decreases as the wing flexion increases, in agreement with the hypothesis proposed in Zhao *et al* (2010).

To further test the hypothesis that camber influences aerodynamic forces via modulation of leading edge vorticity, we directly compared the effect of camber on leading edge vorticity using wings of the same material but three cambers— negative, near zero and zero. These were generated by placing a single wing vein at 20° (for negative camber; inset in figure 3(*a*)), 40° (for almost zero camber; figure 3(*b*)) and 60° (for zero camber; figure 3(*c*)) from the leading edge spar. Using the same models, we have previously shown that the reinforcement of flexible wings with veins greatly augments its ability to generate force, as evident from the polar plots reproduced from Zhao *et al* (2010) (figure 3(*a*)). The measured mean lift force coefficients for 20°, 40° and 60° models respectively at 45° wing angle of attack were 1.1, 1.4 and 1.5 respectively.

As predicted by the hypothesis, these differences were reflected in magnitude of leading edge vorticity, which was minimum for the wing with most negative camber, intermediate for 40° and maximum for 60° veins, as predicted by the hypothesis (upper panels, figures 3(*b*)–(*d*)).

## Discussion

### *Leading edge vorticity as an indicator of aerodynamic performance*

Previous pieces of research have indicated that the leading edge vorticity plays an important role in lift generation in a flapping wing (Maxworthy 1979, Ellington *et al* 1996, Birch *et al* 2004).

This vortex was initially identified on a model flinging wing by Maxworthy (1979), who proposed that it must also exist on flapping wings of insects. Using smoke visualization techniques, Ellington *et al* (1996) identified the leading edge vortex in both model and insect wings and quantified the strength of the leading edge vortex to show that it was strong enough to explain the high lift coefficients. They also noted that the leading edge vortex was stabilized by a strong spiral (axial) flow from the base to the tip of the wing and argued that this may help in stabilizing the leading edge vorticity on a flapping or revolving wing. An alternative hypothesis, proposed by Birch and Dickinson (2001) using DPIV, argued that although the leading edge vortex stability appears to be a common feature of all revolving airfoils, the precise mechanism of stabilization of leading vortices may depend on the Reynolds numbers. Specifically, they did not observe

an axial flow in the case of a revolving airfoil at $Re \sim 100$ as was the case for revolving airfoils at $Re \sim 1000$. More recently, Lentink *et al* (2009) conducted a detailed study to examine the key processes that underlie stability of the leading edge vortex at different values of Reynolds and Rossby numbers. Their study shows that the leading edge vortex stability is mediated by centripetal and Coriolis accelerations at low Rossby numbers, but angular accelerations at high Rossby numbers. This study also identified a range of scales at which the LEV mediated high-lift augmentation could operate. Indeed, several pieces of research have now described stable leading edge vortices the flapping flight in diverse biological scales including insects (Ellington *et al* 1996, Srygley and Thomas 2002), birds (Warrick *et al* 2005), bats (Muijres *et al* 2008), fins of fish (Videler *et al* 2004, Lu and Shen 2008) and also rotating plant seeds (Lentink *et al* 2009). Together, these studies make a strong case for the importance of leading edge vortices in flapping flight.

Regardless of the exact mechanism of leading edge vortex stabilization, the reattachment of flow over the upper surface of the wing indicates that the assumption that Kutta condition is valid for airfoils flapping at high angles of attack in revolving airfoils may be justified. Indeed, this flow feature appears to be intimately connected with the size and strength of the leading edge vorticity. If this hypothesis is true, then subtle alterations of the trailing edge kinematics should cause correlated modulation of the magnitude of leading edge vorticity, and hence also the magnitude of the aerodynamic forces. The current study thus addresses the following two questions. First, how do forces vary when the magnitude of leading edge vorticity changes? Second, how does leading edge vorticity vary in response to alterations in trailing edge kinematics? The experimental setup described here allowed us to simultaneously measure aerodynamic forces and flows on a flapping wing. By using a suite of wings with varying aerodynamic flexibility as well as vein-reinforced wings, we were able to experimentally manipulate trailing edge flexibility and alter the magnitude of the leading edge vortex to examine its influence on aerodynamic forces.

One key finding of this study is that magnitude of the leading edge vorticity correlates well with the aerodynamic forces generated by the flapping wing and is thus a good indicator of the aerodynamic performance of flapping wings during the translational phase of flapping. This is in accordance with the findings of Ellington *et al* (1996), which also implicated the leading edge vortex as a key determinant of aerodynamics forces. A second finding of this study is that trailing edge flexion influences the magnitude of leading edge vorticity. A hypothesis to explain this finding was proposed in Zhao *et al* (2010) and similar to those reproduced here in figures 3(*b*)–(*d*) (top panels). Thus, similar to the ailerons in conventional fixed wing aircrafts, trailing edge flexion can be used to modulate the leading edge vorticity and forces. This hypothesis further implies that the effect of trailing edge flexion on the leading edge vorticity is primarily quasi-static. This would suggest that in case of a dynamically flexing and flapping wing, the instantaneous camber rather than dynamic changes in the camber are a key determinant of

the instantaneous forces on the wing (but also see Mountcastle and Daniel 2010). If true, the flexible wing realigns primarily to minimize shear due to the relative motion of the fluid over the upper and lower surfaces, and the trailing edge sheds very little vorticity. The leading edge vorticity thus assumes a magnitude that ensures the maintenance of Kutta condition.

Under what conditions would the dynamics of flexion become important? Although dynamic flexion may not play a role in the experiments described here as the frequency of flapping greatly exceeds the flexion frequency, this may not be true at values of flexion frequency that are comparable to or higher than the flapping frequency. We are currently planning experiments to determine the flapping-flexion regimes where dynamic flexion becomes significant.

## References

Acheson D 1990 *Elementary Fluid Dynamics* (Oxford: Oxford University Press)

Birch J M and Dickinson M H 2001 Spanwise flow and the attachment of the leading-edge vortex on insect wings *Nature* **412** 729–33

Birch J M *et al* 2004 Force production and flow structure of the leading edge vortex on flapping wings at high and low Reynolds numbers *J. Exp. Biol.* **207** 1063–72

Dickinson M H and Gotz K G 1993 Unsteady aerodynamic performance of model wings at low Reynolds-numbers *J. Exp. Biol.* **174** 45–64

Dickinson M H, Lehmann F O and Sane S P 1999 Wing rotation and the aerodynamic basis of insect flight *Science* **284** 1954–60

Ellington C P 1984a The aerodynamics of hovering insect flight: VI. Lift and power requirements *Phil. Trans. R. Soc.* A **305** 145–81

Ellington C P 1984b The aerodynamics of hovering insect flight: III. Kinematics *Phil. Trans. R. Soc.* B **305** 41–78

Ellington C P *et al* 1996 Leading-edge vortices in insect flight *Nature* **384** 626–30

Gordon J E 1978 *Structures: Or Why Things Don't Fall Down* (New York: Penguin)

Lentink D *et al* 2009 Leading-edge vortices elevate lift of autorotating plant seeds *Science* **324** 1438–40

Liu H and Kawachi K 1999 A numerical study of undulatory swimming *J. Comput. Phys.* V **155** 223–47

Lu Y and Shen G X 2008 Three-dimensional flow structures and evolution of the leading-edge vortices on a flapping wing *J. Exp. Biol.* **211** 1221–30

Maxworthy T 1979 Experiments on the Weis-Fogh mechanism of lift generation by insects in hovering flight *J. Fluid Mech.* **93** 47–63

Mountcastle A M and Daniel T L 2010 Aerodynamic and functional consequences of wing compliance *Exp. Fluids* **46** 873–82

Muijres F T *et al* 2008 Leading-edge vortex improves lift in slow-flying bats *Science* **319** 1250–3

Ramamurti R and Sandberg W C 2002 A three-dimensional computational study of the aerodynamic mechanisms of insect flight *J. Exp. Biol.* **205** 1507–18

Sane S P 2001 The aerodynamics of flapping wings *PhD Thesis* Department of Integrative Biology, University of California, Berkeley, USA

Sane S P and Dickinson M H 2001 The control of flight force by a flapping wing: lift and drag production *J. Exp. Biol.* **204** 2607–26

Sane S P 2003 The aerodynamics of insect flight *J. Exp. Biol.* **206** 4191–208

Srygley R B and Thomas A L 2002 Unconventional lift-generating mechanisms in free-flying butterflies *Nature* **420** 660–4

Videler J J *et al* 2004 Leading-edge vortex lifts swifts *Science* **306** 1960–2

Warrick D R *et al* 2005 Aerodynamics of the hovering hummingbird *Nature* **435** 1094–7

Zhao L *et al* 2010 Aerodynamic effects of flexibility in flapping wings *J. R. Soc. Interface* **7** 485–97